Oncogenic KRAS Induces an Intrinsic Immune Response by Reprogramming the Noncoding Transcriptome

Haley Halasz,[1] Lila Whitehead,[1] David Carrillo,[1] Erin LaMontange,[1]
Eejung Kim,[2,3] Shivani Malik,[4] Eric Collisson,[4] Angela Brooks,[1,5,6] Georgi Marinov,[7]
and Daniel H. Kim[1,5,6,8,9,10,*]

[1]Department of Biomolecular Engineering, University of California Santa Cruz, Santa Cruz, CA 95064 USA
[2]Broad Institute of MIT and Harvard, Cambridge, MA 02142 USA
[3]Department of Medical Oncology, Dana-Farber Cancer Institute, Boston, MA 02215, USA
[4]Department of Medicine, University of California San Francisco, San Francisco, CA 94158, USA
[5]UC Santa Cruz Genomics Institute
[6]Center for Molecular Biology of RNA
University of California Santa Cruz, Santa Cruz, CA 95064 USA
[7]Department of Genetics, Stanford University School of Medicine, Palo Alto, CA 94305, USA
[8]Institute for the Biology of Stem Cells
[9]California Institute for Quantitative Biosciences
University of California Santa Cruz, Santa Cruz, CA 95064 USA

[10]Lead Contact
*Correspondence: daniel.kim@ucsc.edu

SUMMARY

Oncogenic KRAS is a potent initiator of tumorigenesis, yet its nascent effects on the noncoding genome are incompletely understood. Here, we report that oncogenic KRAS dynamically reprograms the transcriptome by modulating the expression of novel long noncoding RNAs, microRNA genes, and human-specific endogenous retroviral RNAs. Endogenous retroviral transcripts activated by mutant KRAS induce viral mimicry in lung epithelial cells undergoing transformation, as evidenced by the upregulation of DExD/H box genes and interferon-stimulated genes. Single-cell transcriptome analysis indicates extensive heterogeneity in the expression of interferon-induced genes, while revealing a core set of coordinately regulated genes that are most highly expressed at intermediate stages of cellular transformation. Moreover, early activation of the immunosuppressive CD274 (PDL1) is a key molecular event stimulated by mutant KRAS. Our findings highlight a complex cell-intrinsic immune response during KRAS-driven transformation and reveal novel, tissue-specific RNA signatures of the earliest stages of cancer formation.

KEYWORDS

KRAS, intrinsic immunity, long noncoding RNA, transcriptome, human endogenous retrovirus, cancer, microRNA, reprogramming

HIGHLIGHTS

- Oncogenic KRAS induces the expression of intrinsic immune response genes
- Human-specific transposon sequences are upregulated by mutant KRAS
- Tissue-specific long noncoding RNAs are expressed upon KRAS activation
- A novel lincRNA SPECTER is regulated by KRAS and controls IL8 expression

INTRODUCTION

Cancers with oncogenic KRAS mutations are responsible for about one million deaths throughout the world each year (Simanshu et al., 2017). Extensive genomic studies have revealed that approximately a third of lung adenocarcinomas, the leading cause of cancer death, contain mutations in KRAS (Cancer Genome Atlas Research, 2014). However, a comprehensive understanding of the nascent stages of KRAS-driven tumorigenesis remains incomplete.

Genome-wide studies have shown that the vast majority of the human genome is transcribed (Djebali et al., 2012), giving rise to diverse classes of noncoding RNAs (Cech and Steitz, 2014). These include microRNAs (Johnson et al., 2005), small nucleolar RNAs (Siprashvili et al., 2016), and long noncoding RNAs (lncRNAs) (Kim et al., 2015; Kotake et al., 2016; Zhang et al., 2017) that have been implicated in RAS signaling pathways. Moreover, over 50,000 lncRNAs have been found in the human genome (Iyer et al., 2015), but only a small fraction of lncRNAs are known to be involved in cancer (Schmitt and Chang, 2016).

In addition to known functional classes of noncoding RNAs, almost half of human genome is comprised of repetitive sequences derived from transposable elements (TEs) (Lander et al., 2001). Exposing cancer cells to DNA-demethylating agents activates the expression of a specific class of TEs known as endogenous retroviruses (ERVs), leading to viral mimicry and an interferon response (Chiappinelli et al., 2015; Roulois et al., 2015). Interferon signaling also causes cancer cells to resist immune checkpoint blockade (ICB), and this resistance can be mediated by the immunosuppresive CD274 (PDL1) (Benci et

al., 2016). Taken together, these observations suggest multilayered interactions between immune response genes and the various types of noncoding RNAs that are aberrantly expressed in cancer cells.

Here, we characterized dynamic changes in the noncoding transcriptome in a well-established in vitro model of KRAS-driven primary human airway epithelial cell transformation (Lundberg et al., 2002). We identified ERVs and long terminal repeat (LTR) elements, microRNA genes, and lncRNA genes that participate in a complex network of intrinsic immune response genes induced by mutant KRAS.

RESULTS

Transcriptome Analysis of Transforming Lung Epithelial Cells

We performed RNA sequencing (RNA-seq) of airway epithelial cells (AALEs) at various timepoints of transformation to determine how the transcriptome was responding to oncogenic KRAS mutation at glycine 12 (G12), which is frequently mutated in lung adenocarcinomas (Figure 1A). We introduced plasmids containing mutant KRAS(G12V) and a puromycin resistance gene into AALEs and grew them under puromycin selection for 5, 14, and 21 days. Additionally, we compared these transforming cells to stable AALE cell lines that had integrated a mutant KRAS(G12D) plasmid or the plasmid backbone alone as a control. For each cell type, we generated RNA-seq libraries from 3 biological replicates and performed differential expression analysis to identify genes that were significantly differentially expressed (Figure 1B). Thousands of genes were upregulated

at each timepoint and in the stable KRAS mutant cells, and we focused on the upregulated genes to identify pathways that were being turned on by oncogenic KRAS signaling.

When we examined the set of genes that were upregulated across all transformation timepoints, as well as in the stable KRAS mutant cells, we identified a core set of 129 genes that were significantly overexpressed across all 12 biological samples that we sequenced (Figure 1C). We then performed gene ontology (GO) analysis on the upregulated genes at each stage of transformation to uncover common pathways that were activated by mutant KRAS (Figure 1D). At the earliest timepoints (Day 5, Day 14), we found statistically significant enrichment of the GO terms 'RNA processing' and 'ncRNA processing', but these terms did not appear at later stages of transformation. The 'ncRNA processing' GO term contained several genes involved in RNA interference (RNAi) and the microRNA pathway (AGO2, AGO4, DGCR8, DROSHA), as well as multiple DEAD box RNA helicase proteins (DDX21, DDX51, DDX52) and components of the exosome complex (EXOSC3, EXOSC4, EXOSC6, EXOSC7), indicating that regulatory RNA and RNA processing pathways are activated concurrently during early stages of cellular transformation.

The GO term 'embryo development' was also significantly enriched during our transformation timecourse experiments, highlighting several genes implicated in KRAS-driven cancers, included YAP1 (Kapoor et al., 2014; Shao et al., 2014), NOTCH1 (Licciulli et al., 2013), and LIF (Corcoran et al., 2011). Genes involved in the 'immune response' and 'response to virus' were also represented across all stages that we examined, reinforcing their broadly involvement in KRAS-mediated transformation.

Mutant KRAS Induces Viral Mimicry

To identify the core set of intrinsic immune response genes that are overexpressed in mutant KRAS cells, we examined the common set of 129 genes that were significantly upregulated at all stages of transformation (Figure 2A). Several of these genes were previously shown to be induced upon DNA demethylation, including DDX58, IFIH1, ISG15, IFI44, IFI27, HLA-C, IFI44L, and STAT1 (Chiappinelli et al., 2015; Roulois et al., 2015). Other genes that we identified have not been previously linked to cancer, such as C19orf66, an antiviral gene involved in repressing Dengue virus (Suzuki et al., 2016), THEMIS2, a scaffold gene that regulates Toll-like receptor signaling (Peirce et al., 2010), and DDX60L, an interferon-stimulated gene involved in repressing hepatitis C virus (Grunvogel et al., 2015).

Mutant KRAS also induced several other interferon-related genes, including IFI6, IFIT1, and IFIT3, as well as IFIT5 and IFI35, which have not been previously implicated in lung cancers. We sought to discover the endogenous TEs that were inducing the expression of interferon-related genes and found that all of the activated ERVs and LTRs were either human-specific (7 out of 9) or primate-specific (2 out of 9), indicating that viral mimicry is induced by endogenous TEs that have only recently incorporated into the human genome (Figure 2B). At early timepoints (Day 5), we observed significant upregulation of LTR12C, LTR12D, and LTR43_I elements, and at later timepoints (Day 21), HERVK11I and HERVL elements were the most significantly activated. Coverage plots for HERVK11I and HERKVL showed that the 3' ends of the consensus elements

were upregulated (Figure 2C), and this region encodes the envelope (env) protein, which is thought to contain an immunosuppressive domain (Gonzalez-Cao et al., 2016).

Mutant KRAS cells also significantly upregulated the interferon-inducible RNA helicase DDX60 (Figure 2D), as well as the immunosuppressive CD274 (PDL1) at the earliest timepoints of cellular transformation (Figure 2E). CD274 (PDL1) exhibited both nuclear and perinuclear localization in KRAS mutant cells, and previous reports indicate that its nuclear localization is associated with poor survival in cancer patients (Satelli et al., 2016). Taken together, our results reveal that multiple immunosuppressive pathways are activated by mutant KRAS.

Upregulation of MicroRNA Pathway Genes by Mutant KRAS

Due to the enrichment of the 'ncRNA processing' GO term during KRAS-driven transformation, we examined the expression of microRNA pathway genes, as well as primary microRNA transcript expression. In addition to AGO2 and AGO4, AGO1 and AGO3 were upregulated to a lesser extent (Figure 3A). AGO2 exhibited perinuclear localization in mutant KRAS cells, and previous studies have shown that AGO2 can associate with KRAS to mediate cellular transformation (Shankar et al., 2016). Kaplan-Meier analysis of The Cancer Genome Atlas (TCGA) pan-cancer (pancan) RNA-seq data showed that high AGO2 expression was significantly correlated with poor survival (P-value = 0.000) when examined across all cancers (Figure 3). When we examined the expression of microRNA host genes (HG), 9 genes were significantly downregulated, while 4 genes were significantly upregulated (Figure 3D). Two downregulated microRNA

HGs, MIR4458HG (Figure 3E) and MIR99AHG (Figure 3F) were significantly correlated with poor survival when their expression levels were low across all cancer types examined.

Mutant KRAS Activates Tissue-Specific Long Noncoding RNAs

Given the prevalence of lncRNAs genes in the human genome, we investigated how mutant KRAS affected the expression of lncRNAs. Hundreds of lncRNAs were significantly perturbed by mutant KRAS (Figure 4A) at the earliest stages of AALE cell transformation. We examined human embryonic kidney (HA1E) cells that stably expressed mutant KRAS(G12V) to discriminate between lncRNAs that were broadly expressed in response to mutant KRAS versus lncRNAs that were more specifically induced in cells from a given tissue type. The majority of lncRNAs that were activated in each cell type were most highly expressed in only that particular cell type (Figure 4B). These results reveal that KRAS-induced lncRNA signatures are tissue-specific.

Mutant KRAS also activates several well-characterized and more broadly expressed lncRNAs, such as NEAT1, MALAT1, XIST, and TSIX, as well as a novel lncRNA which we refer to as SPECTER (also known as LINC00707) for SPECific Transcript Expressed by Ras mutant cells (Figure 4C). Given the connection between X-chromosome inactivation and cancer (Lee and Bartolomei, 2013), we looked at XIST levels more carefully and found that coverage of the XIST transcript was uniformly down in mutant KRAS cells (Figure 4D), and we also observed the loss of XIST clouds in a subset of mutant KRAS cells (Figure 4E). Across all female cancer patients in the TCGA

PANCAN dataset, low levels of XIST were significantly correlated with poor survival (Figure 4F).

SPECTER: A Novel LncRNA that Regulates NF-kB signaling

We next sought to understand how SPECTER might be involved in KRAS-driven transformation. SPECTER is expressed in both the nuclear and cytoplasmic compartments (Figure 5A) and is uniformly upregulated in mutant KRAS cells based on UCSC Genome Browser coverage tracks (Figure 5B). Across all cancers examined, high SPECTER expression significantly correlates with poor survival (P-value = 0.000) (Figure 5C). We performed loss-of-function experiments using two different small interfering RNAs (siRNAs) that target SPECTER and identified an overlapping set of genes that were significantly downregulated upon loss of SPECTER expression (Figure 5D). We looked for potential protein-protein interactions among the downregulated genes using the STRING database and found significant enrichment of genes involved in NF-kB signaling (CFLAR, CXCL8 (IL8), CXCL2, TAB3, XIAP, LTBR, TNFAIP3, TRAF2) (Figure 5E), suggesting a model for the role of SPECTER in KRAS-driven transformation (Figure 5F).

Single-Cell RNA-Seq Reveals Heterogeneity in Intrinsic Immune Response Genes

To understand how individual cells were being transforming by mutant KRAS, we performed single-cell RNA-seq at defined stages of cellular transformation (Day 14 and stable KRAS mutants) (Figure 6A). Cluster analysis revealed that there were 5 major clusters within the single cell data, and the majority of Day 14 mutant KRAS cells were

located in cluster 3 (Figure 6B). Cluster 3 cells showed significant overexpression of the interferon-related genes ISG15, IFITM3, and IFI27 (Figure 6C and 6D). Moreover, high levels of IFI27 and IFITM3 were significantly correlated with poor survival across all cancers examined (P-value = 0.000 for both) (Figure 6E).

Taken together, these results highlight the prominent role of interferon-related genes during KRAS-driven cellular transformation and suggest a model (Figure 7) whereby mutant KRAS activates endogenous TEs and noncoding RNAs that elicit and interact with a complex intrinsic immune response during the nascent stages of cancer formation.

AUTHOR CONTRIBUTIONS

Conceptualization, D.H.K.; Methodology, H.H. and D.H.K.; Software, G.M.; Investigation, H.H., L.W., D.C., E.L., and E.K.; Resources, S.M., E.C., and A.B.; Writing, D.H.K; Visualization, G.M. and D.H.K; Supervision, D.H.K.; Funding Acquisition, D.H.K.

FIGURE LEGENDS

Figure 1. Transcriptome Profiling of Mutant KRAS-Driven Transformation

(A) Schematic diagram of time-course experiments to identify genes involved in KRAS-mediated transformation of primary human airway epithelial cells.

(B) Heatmaps of differentially expressed genes between wild-type (WT) KRAS and mutant KRAS cells at each timepoint.

(C) Venn diagram of significantly upregulated genes between WT KRAS and mutant KRAS cells at each timepoint.

(D) Gene ontology (GO) analysis of significantly enriched GO terms for upregulated genes between WT KRAS and mutant KRAS cells at each timepoint.

Figure 2. Mutant KRAS Induces Immune Response Genes and Human-Specific TEs

(A) Heatmap of a common set of 129 significantly upregulated genes between WT KRAS and mutant KRAS cells across all timepoints. Shown here are their expression levels in WT KRAS and Day 21 mutant KRAS cells.

(B) Heatmap of significantly upregulated human- or primate-specific transposable elements (TEs) between WT KRAS and mutant KRAS cells at each timepoint.

(C) Coverage plots for human-specific HERVK11I and HERVL consensus elements in WT KRAS and Day 21 mutant KRAS cells.

(D and E) Immunofluorescence analysis of DDX60 and CD274 (PDL1) expression in WT KRAS and mutant KRAS cells.

Figure 3. Mutant KRAS Stimulates MicroRNA Pathway Activity

(A) Heatmap of microRNA pathway gene expression in WT KRAS and mutant KRAS cells.

(B) Immunofluorescence analysis of AGO2 expression in WT KRAS and mutant KRAS cells.

(C) Kaplan-Meier survival analysis for AGO2 expression using The Cancer Genome Atlas (TCGA) Pan-Cancer (PANCAN) RNA sequencing data.

(D) Heatmap of differentially expressed primary microRNA transcripts in WT KRAS and mutant KRAS cells.

(E and F) Kaplan-Meier survival analysis for MIR4458HG and MIR99AHG expression using TCGA PANCAN data.

Figure 4. Tissue-Specific Enrichment of Long Noncoding RNAs Activated by Mutant KRAS

(A) Scatterplot of differentially expressed long intergenic noncoding RNAs (lincRNAs) in WT KRAS and mutant KRAS cells.

(B) Heatmap of differentially expressed lincRNAs in WT KRAS and mutant KRAS kidney (HA1E) cells and lung (AALE) cells.

(C) Heatmap of specific lincRNA expression in WT KRAS and mutant KRAS cells.

(D) UCSC Genome Browser tracks showing coverage of the XIST gene in WT KRAS and mutant KRAS cells.

(E) Single-molecule RNA fluorescence in situ hybridization (FISH) for XIST in WT KRAS and mutant KRAS cells. Scale bars indicate 10um.

(F) Kaplan-Meier survival analysis for XIST expression in females using TCGA PANCAN data.

Figure 5. Mutant KRAS-Activated LncRNA SPECTER regulates NF-kB Signaling

(A) Single-molecule RNA FISH for SPECTER in WT KRAS and mutant KRAS cells. Scale bars indicate 10um.

(B) UCSC Genome Browser tracks showing coverage of the SPECTER gene in WT KRAS and mutant KRAS cells.

(C) Kaplan-Meier survival analysis for SPECTER expression using TCGA PANCAN data.

(D) Heatmap of overlapping differentially expressed genes in airway epithelial cells transfected with control siRNA or two different siRNAs targeting SPECTER.

(E) Heatmap of differentially expressed NF-kB signaling genes in airway epithelial cells transfected with control siRNA or two different siRNAs targeting SPECTER.

(F) Model for SPECTER function in regulating mutant KRAS-driven NF-kB signaling.

Figure 6. Single-Cell RNA Sequencing Reveals Heterogeneity in Immune Response Gene Induction by Mutant KRAS

(A) Transcriptome analysis and visualization of 2,342 WT KRAS, 2,062 Day 14 Mutant KRAS, and 1,504 Stable Mutant KRAS cells by t-distributed stochastic neighbor embedding (tSNE).

(B) Heatmap of all genes expressed in individual clusters of single cells.

(C) Heatmap of differentially expressed genes enriched in cluster 3.

(D) ISG15, IFI27, and IFITM3 expression in single cells.

(E) Kaplan-Meier survival analysis for IFI27 and IFITM3 expression using TCGA PANCAN data.

Figure 7. Model for Mutant KRAS-Mediated Transformation

STAR METHODS

Experimental Model and Subject Details

Cell Lines

The wild-type female AALE cell line was provided by Scott Randell's Lab at University of North Carolina. The female AALE stable cell lines pBABE-mCherry Puro and pBABE-FLAG-KRAS(G12) Zeo was provided by Eric Collisson's Lab at University of California, San Francisco. Both lines were cultured in SABM Basal Medium (Lonza SABM basal medium) with added supplements and growth factors (Lonza SAGM SingleQuot Kit Suppl. & Growth Factors). AALE cell lines were maintained using Lonza's ReagentPack subculture reagents and standard tissue culture procedures. The HA1E cells were derived from female human embryonic kidney cells in Bill Hahn's Lab at Dana Farber Cancer Institute. Wild-type HA1E cells and the HA1E pLX317-KRAS(G12) stable cell line were cultured in MEM-alpha (Invitrogen) with 10% FBS (Sigma) and 1% penicillin/streptomycin (Gibco). All cell lines tested negative for mycoplasma.

Method Details

Plasmids and siRNAs

pBABE-KRAS(G12) Puro was purchased from Addgene (plasmid #9052). SPECTER/LINC00707 siRNAs were designed and purchased from IDT (see key resource table for sequence details).

https://www.addgene.org/kits/boehm-target-accelerator-cancer-collection/

Transfections

100mm dishes of 80% confluent AALE cells were transfected with 12ug of pBABE-KRAS(G12) Puro plasmid using Invitrogen Lipofectamine 2000 DNA transfection reagent and protocol. After 24hrs, the medium was replaced with SAGM supplemented with 2ug/ml of puromycin. Transfected cells were kept under puromycin selection for 5, 14, and 21 days. Cells were trypsinized and harvested by centrifugation at 300 g x 3 minutes for RNA extraction at each time point respectively. For siRNAs, 12-well plates of 80% confluent wild-type AALE cells were reverse transfected with 25pmol of siRNA targeting LINC00707/SPECTER for knockdown by RNAi, using Invitrogen Lipofectamine RNAiMAX reagent and protocol. Cells were kept in the transfection reagent-containing medium for 24hrs. After 24hrs the cells were trypsinized and harvested by centrifugation at 300 g x 3 minutes for RNA extraction.

RNA Isolation & Purification

For AALE cell lines, bulk RNA was isolated from cells using Quick-RNA MiniPrep Kit (Zymo) and quantified via NanoDrop-8000 Spectrophotometer. For HA1E cell lines, bulk RNA was isolated using RNeasy Mini Kit (Qiagen) and quantified via Qubit RNA BR assay kit (Thermo).

qPCR

cDNA was transcribed from 1ug RNA using iScript cDNA Synthesis Kit (Bio-Rad) according to manufacturer protocol. cDNA was diluted 1:6 and run with iTaq Universal

SYBR Green Supermix (Bio-Rad) on ViiA 7 Real-Time PCR System according to Supermix manufacturer protocol.

Library Preparation for Bulk RNAseq

For AALE cell lines, 1ug of total RNA was used as input for the TruSeq Stranded mRNA Sample Prep Kit (Illumina) according to manufacturer protocol. Library quality was determined through the High Sensitivity DNA Kit on a Bioanalyzer 2100 (Agilent Technologies). For HA1E cell lines, 1ug of total RNA was used for mRNA enrichment with Dynabeads mRNA DIRECT kit (Thermo). First strand cDNA was generated with AffinityScript Multiple Temperature reverse transcriptase with oligo dT primers. Second strand cDNA was generated with mRNA Second Strand Sythesis Module (New England Biolab). DNA was cleaned up with Agencourt AMPure XP beads twice. Qubit dsDNA High Sensitivity Assay was used for concentration measurement. 1ng of dsDNA was further subjected to library preparation with Nextera XT DNA sample prep kit (Illumina) per manufacturer instructions. Library size distribution was confirmed with Bioanalyzer (Agilent). Multiplexed libraries were sequenced as NextSeq500 75PE runs.

Library Preparation for Single Cell RNAseq

For single cell RNAseq, $1x10^6$ cells were harvested and re-suspended in 1mL 1X PBS/0.04% BSA (1000 cells/ul) according to the cell preparation guidelines in the 10X Genomics Chromium Single Cell 3' Reagent Kit User Guide. GEMs were generated from an input of 3,500 cells. We used the 10X Genomics Chromium Single Cell 3' Reagent

Kits version 2 for both the GEM generation and subsequent library preparation and followed the manufacturer's reagent kit protocol. Quantification of all RNAseq libraries was performed by QB3 at UC Berkeley. All AALE cell line RNAseq libraries were sequenced as HiSeq4000 100PE runs.

Immunoblotting

Cells were lysed in a modified RIPA buffer (Sigma) and lysates were centrifuged at 13,000 rpm for 10 min to obtain post-nuclear supernatants for determination of protein concentration by Pierce BCA protein assay (Thermo). Twenty micrograms of protein was separated by SDS-PAGE and transferred to 0.45 μm PVDF membranes (Millipore) in transfer buffer (25 mM Tris, 200 mM glycine, 20% methanol). Membranes were blocked for 1 hour in 5% milk in Tris-buffered saline (TBST) (20 mM Tris-Cl, pH 7.4 with 0.1% Tween 20) and then incubated with primary antibodies overnight at 4 °C . Primary antibodies used: Beta Actin, Phospho-ERK, KRAS (1:2000, 1:1000, 1:1000 dilutions respectively). After washing three times for ten minutes with TBST, membranes were incubated with secondary antibodies (HRP conjugated Goat anti Rabbit or Goat anti Mouse, Biorad, 1:10,000 dilutions) for 1 hour at room temperature. Secondary antibodies were washed from the membrane three times for ten minutes with TBST and developed with luminol-peroxide reagent (Biorad). Chemilluminesence imaging was performed using a multi-image light cabinet (Biorad) with Image Lab software (Biorad).

Immunofluorescence

All cells were grown on coverslips for the immunofluorescence protocol. Cells were rinsed with 1x PBS prior to fixation in 4% paraformaldehyde (Thermo) for ten minutes. After fixation, cells were washed three times with PBST (1x PBS, 0.1% Triton X-100) for 5 minutes. Cells were then blocked in PBST containing 5% BSA for 1 hour at room temperature. Cells were again rinsed three times with PBST for 5 minutes and then incubated with primary antibodies in PBST with 3% BSA overnight. Primary antibodies used were: mouse anti-CD47, mouse anti-Ago2, rabbit anti-PDL-1, rabbit anti-DDX60, rabbit anti-KRAS (1:100, 1:1000, 1:500, 1:100, 1:500 dilutions respectively) . After washing three times with PBST five minutes each, cells were incubated with secondary antibodies (Alexa Fluor 568 and Alexa Fluor 647) for 1 hour at room temperature in PBST with 3% BSA. Cells were then washed twice with 1x PBST and counterstained with DAPI (Thermo) for five minutes. After counterstaining with DAPI, cells were rinsed twice with 1x PBS for 5 minutes and were mounted onto microscope slides using Vectashield mounting medium. All images were captured using a Zeiss Axioimager fluorescent microscope.

Imaging and Image Processing

All images were processed via 3D blind deconvolution using AutoQuant x3 software and subsequent image capture was performed using Imaris image processing software.

Single Molecule RNA FISH

Cells were grown on glass coverslips and fixed with 4% paraformaldehyde. After fixation cells were permeabilized in 70% ethanol. All subsequent steps were performed as per manufacturer instructions for the FISH probes targeting: MALAT-1, NEAT-1, XIST, and LINC00707/SPECTER (Biosearch Technologies).

KEY RESOURCES TABLE

REAGENT or RESOURCE	SOURCE	IDENTIFIER
Antibodies		
Anti -DDX60	Sigma	sab3500806
Anti- EIFC2	Sigma	wh002716m1
Anti- KRAS	ProteinTech	12063-1-AP
Anti- Beta Actin	Abcam	ab8227
Anti- Phospho-MAPK	Millipore Sigma	mabs71
Anti- CD47	NeoMarkers	b6h12.2
Anti- PDL1	Abcam	ab213524
Goat anti rabbit HRP	Abcam	ab6721
Goat anti mouse HRP	Abcam	ab6789
Donkey anti Rabbit Alexa Fluor 568	Abcam	ab175470
Donkey anti Mouse Alexa Fluor 647	Abcam	ab150107

Chemicals, Peptides, and Recombinant Proteins		
RIPA Buffer	Sigma	R0278
SigmaFast Protease Inhibitor Tablets	Sigma	S8820
Vectashield Hard Set	Vector Laboratories	H-1400
DAPI	Invitrogen	D1306
Lipofectamine 2000	LifeTech	Cat. #11668019
Lipofectamine RNAiMAX	LifeTech	Cat. #13778150
Opti-MEM	LifeTech	Cat. #31985062
SAGM Bulletkit	Lonza	Cat. #CC-3118
Reagent Pack Subculture Reagents	Lonza	Cat. #CC-5034
Critical Commercial Assays		
Quick-RNA MiniPrep Kit	Zymo	Cat. #R1055
Quick-cfRNA Serum and Plasma	Zymo	Cat. #R1059
DNase I Set	Zymo	Cat. #E1010
Oligo Clean & Concentrator	Zymo	Cat. #D4060
Qubit RNA HS Assay Kit	Thermo Fisher	Cat. #Q32852
iScript cDNA Synthesis Kit	Bio-Rad	Cat. #1708891
iTaq Universal SYBR Green Supermix	Bio-Rad	Cat. #1725121

TruSeq Stranded mRNA Sample Prep Kit A	Illumina	Cat. #RS-122-2101
TruSeq Stranded mRNA Sample Prep Kit B	Illumina	Cat. #RS-122-2102
High Sensitivity DNA Kit	Agilent Technologies	Cat. #5067-4626
SMART-Seq v4 Ultra Low Input RNA Kit	Takara Bio	Cat. #634888
Plasmid PlusMidi Kit	QIAGEN	Cat. #12943
PureLink Genomic DNA Mini Kit	Invitrogen	Cat. #K1820-01
Qubit dsDNA BR Assay Kit	Thermo Fisher	Cat. #Q32850
Custom Stellaris FISH Probe: LINC00707/SPECTER Quasar 670	Biosearch Technologies	Part#SMF-1065-5007
Stellaris FISH Probe: NEAT1_5 Quasar 570	Biosearch Technologies	Cat. #SMF-2036-1
Stellaris FISH Probe: XIST Quasar 570	Biosearch Technologies	Cat. #SMF-2038-1
Stellaris FISH Probe: MALAT1 Quasar 670	Biosearch Technologies	Cat. #SMF-2046-1
Stellaris RNA FISH Wash Buffer A	Biosearch Technologies	Cat. #SMF-WA1-60
Stellaris RNA FISH Wash Buffer B	Biosearch Technologies	Cat. #SMF-WB1-20

Stellaris RNA FISH Hybridization Buffer	Biosearch Technologies	Cat. #SMF-HB1-10
Deposited Data		
Experimental Models: Cell Lines		
AALE	Scott Randell, UNC	N/A
Stable pBABE-FLAG-KRAS(G12) Zeo AALE	Eric Collisson, UCSF	N/A
Stable pBABE-mCherry Puro AALE	Eric Collisson, UCSF	N/A
Oligonucleotides		
KRAS Forward: GGACTGGGGAGGGCTTTCT	IDT	PCR Primer
KRAS Reverse: GCCTGTTTTGTGTCTACTGTTCT	IDT	PCR Primer
SPECTER Forward: ACCCATCACCTCAACTTTCC	IDT	PCR Primer
SPECTER Reverse: GCTGGCCCTGTTCTATTTACT	IDT	PCR Primer
Beta-actin Forward: TGAAGTGTGACGTGGACATC	IDT	PCR Primer
Beta-actin Reverse: GGAGGAGCAATGATCTTGAT	IDT	PCR Primer
KRAS siRNA 1: CGAUACAGCUAAUUCAGAAUCAUTT	IDT	PCR Primer
KRAS siRNA 2: ACAGGAAGCAAGUAGUAAUUGAUGG	IDT	PCR Primer

SPECTER siRNA 1: CUGAUUUACCUUCCAAUUAUUGUTT	IDT	DsiRNA
SPECTER siRNA 2: GUGGAUAAGACUAACACUGAACCAA	IDT	DsiRNA
Cy3 Transfection Control siRNA	IDT	DsiRNA
Negative Control siRNA	IDT	DsiRNA
Recombinant DNA		
Plasmid: pBABE-KRAS(G12) Puro	Addgene	#9052
Software and Algorithms		
Autoquant X3	Media Cybernetics	
Imaris	Bitplane	
FIJI		

REFERENCES

Benci, J.L., Xu, B., Qiu, Y., Wu, T.J., Dada, H., Twyman-Saint Victor, C., Cucolo, L., Lee, D.S., Pauken, K.E., Huang, A.C.*, et al.* (2016). Tumor Interferon Signaling Regulates a Multigenic Resistance Program to Immune Checkpoint Blockade. Cell *167*, 1540-1554 e1512.

Cancer Genome Atlas Research, N. (2014). Comprehensive molecular profiling of lung adenocarcinoma. Nature *511*, 543-550.

Cech, T.R., and Steitz, J.A. (2014). The noncoding RNA revolution-trashing old rules to forge new ones. Cell *157*, 77-94.

Chiappinelli, K.B., Strissel, P.L., Desrichard, A., Li, H., Henke, C., Akman, B., Hein, A., Rote, N.S., Cope, L.M., Snyder, A.*, et al.* (2015). Inhibiting DNA Methylation Causes an Interferon Response in Cancer via dsRNA Including Endogenous Retroviruses. Cell *162*, 974-986.

Corcoran, R.B., Contino, G., Deshpande, V., Tzatsos, A., Conrad, C., Benes, C.H., Levy, D.E., Settleman, J., Engelman, J.A., and Bardeesy, N. (2011). STAT3 plays a critical role in KRAS-induced pancreatic tumorigenesis. Cancer Res *71*, 5020-5029.

Djebali, S., Davis, C.A., Merkel, A., Dobin, A., Lassmann, T., Mortazavi, A., Tanzer, A., Lagarde, J., Lin, W., Schlesinger, F.*, et al.* (2012). Landscape of transcription in human cells. Nature *489*, 101-108.

Gonzalez-Cao, M., Iduma, P., Karachaliou, N., Santarpia, M., Blanco, J., and Rosell, R. (2016). Human endogenous retroviruses and cancer. Cancer Biol Med *13*, 483-488.

Grunvogel, O., Esser-Nobis, K., Reustle, A., Schult, P., Muller, B., Metz, P., Trippler, M., Windisch, M.P., Frese, M., Binder, M.*, et al.* (2015). DDX60L Is an Interferon-Stimulated Gene Product Restricting Hepatitis C Virus Replication in Cell Culture. J Virol *89*, 10548-10568.

Iyer, M.K., Niknafs, Y.S., Malik, R., Singhal, U., Sahu, A., Hosono, Y., Barrette, T.R., Prensner, J.R., Evans, J.R., Zhao, S.*, et al.* (2015). The landscape of long noncoding RNAs in the human transcriptome. Nat Genet *47*, 199-208.

Johnson, S.M., Grosshans, H., Shingara, J., Byrom, M., Jarvis, R., Cheng, A., Labourier, E., Reinert, K.L., Brown, D., and Slack, F.J. (2005). RAS is regulated by the let-7 microRNA family. Cell *120*, 635-647.

Kapoor, A., Yao, W., Ying, H., Hua, S., Liewen, A., Wang, Q., Zhong, Y., Wu, C.J., Sadanandam, A., Hu, B.*, et al.* (2014). Yap1 activation enables bypass of oncogenic Kras addiction in pancreatic cancer. Cell *158*, 185-197.

Kim, D.H., Marinov, G.K., Pepke, S., Singer, Z.S., He, P., Williams, B., Schroth, G.P., Elowitz, M.B., and Wold, B.J. (2015). Single-cell transcriptome analysis reveals dynamic changes in lncRNA expression during reprogramming. Cell Stem Cell *16*, 88-101.

Kotake, Y., Naemura, M., Kitagawa, K., Niida, H., Tsunoda, T., Shirasawa, S., and Kitagawa, M. (2016). Oncogenic Ras influences the expression of multiple lncRNAs. Cytotechnology *68*, 1591-1596.

Lander, E.S., Linton, L.M., Birren, B., Nusbaum, C., Zody, M.C., Baldwin, J., Devon, K., Dewar, K., Doyle, M., FitzHugh, W.*, et al.* (2001). Initial sequencing and analysis of the human genome. Nature *409*, 860-921.

Lee, J.T., and Bartolomei, M.S. (2013). X-inactivation, imprinting, and long noncoding RNAs in health and disease. Cell *152*, 1308-1323.

Licciulli, S., Avila, J.L., Hanlon, L., Troutman, S., Cesaroni, M., Kota, S., Keith, B., Simon, M.C., Pure, E., Radtke, F.*, et al.* (2013). Notch1 is required for Kras-induced lung adenocarcinoma and controls tumor cell survival via p53. Cancer Res *73*, 5974-5984.

Lundberg, A.S., Randell, S.H., Stewart, S.A., Elenbaas, B., Hartwell, K.A., Brooks, M.W., Fleming, M.D., Olsen, J.C., Miller, S.W., Weinberg, R.A.*, et al.* (2002). Immortalization and transformation of primary human airway epithelial cells by gene transfer. Oncogene *21*, 4577-4586.

Peirce, M.J., Brook, M., Morrice, N., Snelgrove, R., Begum, S., Lanfrancotti, A., Notley, C., Hussell, T., Cope, A.P., and Wait, R. (2010). Themis2/ICB1 is a signaling scaffold that selectively regulates macrophage Toll-like receptor signaling and cytokine production. PLoS One *5*, e11465.

Roulois, D., Loo Yau, H., Singhania, R., Wang, Y., Danesh, A., Shen, S.Y., Han, H., Liang, G., Jones, P.A., Pugh, T.J.*, et al.* (2015). DNA-Demethylating Agents Target Colorectal Cancer Cells by Inducing Viral Mimicry by Endogenous Transcripts. Cell *162*, 961-973.

Satelli, A., Batth, I.S., Brownlee, Z., Rojas, C., Meng, Q.H., Kopetz, S., and Li, S. (2016). Potential role of nuclear PD-L1 expression in cell-surface vimentin positive circulating tumor cells as a prognostic marker in cancer patients. Sci Rep *6*, 28910.

Schmitt, A.M., and Chang, H.Y. (2016). Long Noncoding RNAs in Cancer Pathways. Cancer Cell *29*, 452-463.

Shankar, S., Pitchiaya, S., Malik, R., Kothari, V., Hosono, Y., Yocum, A.K., Gundlapalli, H., White, Y., Firestone, A., Cao, X.*, et al.* (2016). KRAS Engages AGO2 to Enhance Cellular Transformation. Cell Rep *14*, 1448-1461.

Shao, D.D., Xue, W., Krall, E.B., Bhutkar, A., Piccioni, F., Wang, X., Schinzel, A.C., Sood, S., Rosenbluh, J., Kim, J.W.*, et al.* (2014). KRAS and YAP1 converge to regulate EMT and tumor survival. Cell *158*, 171-184.

Simanshu, D.K., Nissley, D.V., and McCormick, F. (2017). RAS Proteins and Their Regulators in Human Disease. Cell *170*, 17-33.

Siprashvili, Z., Webster, D.E., Johnston, D., Shenoy, R.M., Ungewickell, A.J., Bhaduri, A., Flockhart, R., Zarnegar, B.J., Che, Y., Meschi, F.*, et al.* (2016). The noncoding RNAs SNORD50A and SNORD50B bind K-Ras and are recurrently deleted in human cancer. Nat Genet *48*, 53-58.

Suzuki, Y., Chin, W.X., Han, Q., Ichiyama, K., Lee, C.H., Eyo, Z.W., Ebina, H., Takahashi, H., Takahashi, C., Tan, B.H.*, et al.* (2016). Characterization of RyDEN (C19orf66) as an Interferon-Stimulated Cellular Inhibitor against Dengue Virus Replication. PLoS Pathog *12*, e1005357.

Zhang, D., Zhang, G., Hu, X., Wu, L., Feng, Y., He, S., Zhang, Y., Hu, Z., Yang, L., Tian, T.*, et al.* (2017). Oncogenic RAS Regulates Long Noncoding RNA Orilnc1 in Human Cancer. Cancer Res *77*, 3745-3757.

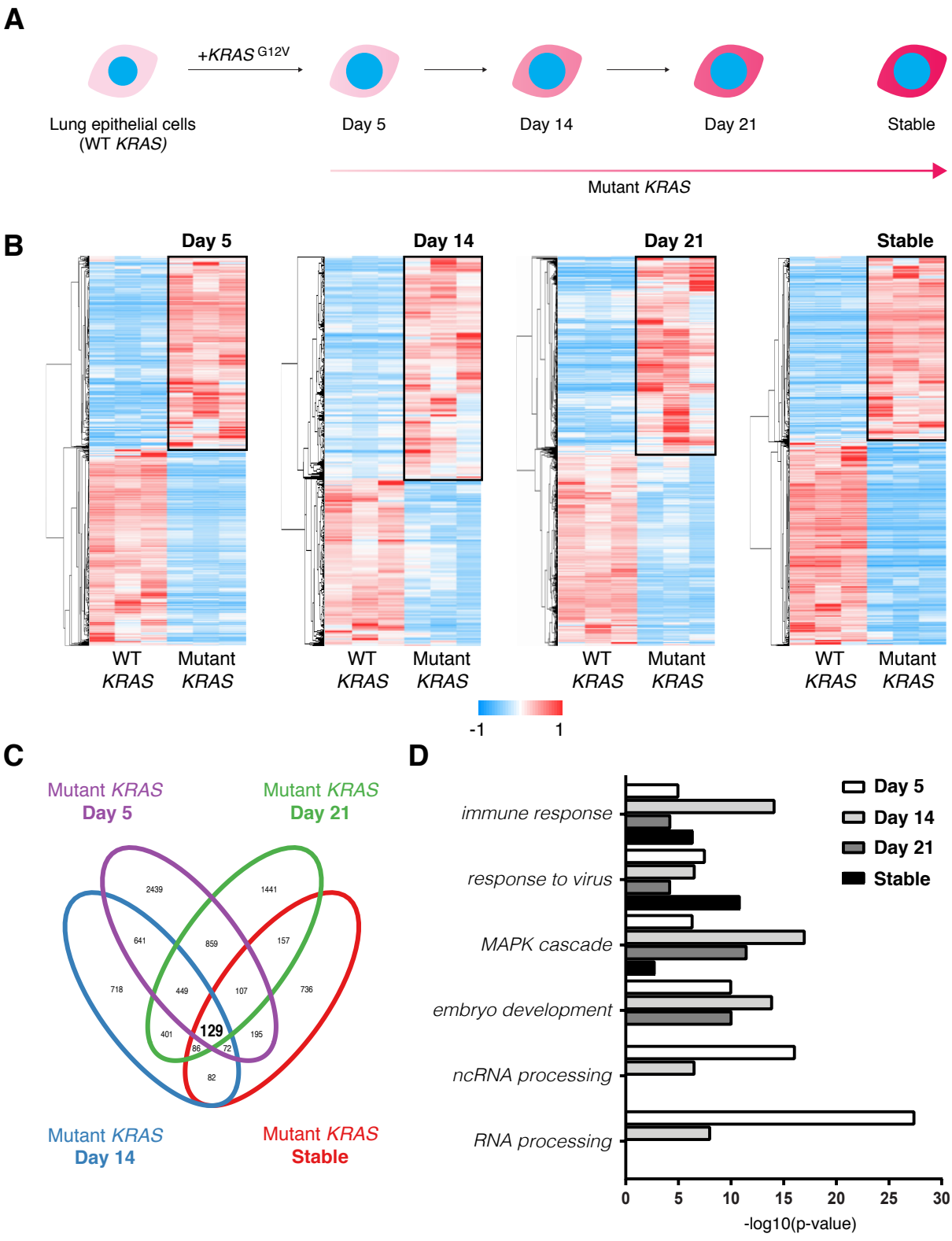
A
+KRAS G12V
Lung epithelial cells
(WT KRAS)
Day 5
Day 14
Day 21
Stable
Mutant KRAS
B
Day 5
Day 14
Day 21
Stable
WT KRAS
Mutant KRAS
-1
1
C
Mutant KRAS
Day 5
Mutant KRAS
Day 21
Mutant KRAS
Day 14
Mutant KRAS
Stable
2439
1441
641
859
157
718
449
107
736
401
129
195
86
72
82
D
immune response
response to virus
MAPK cascade
embryo development
ncRNA processing
RNA processing
Day 5
Day 14
Day 21
Stable
0
5
10
15
20
25
30
-log10(p-value)

Figure 1

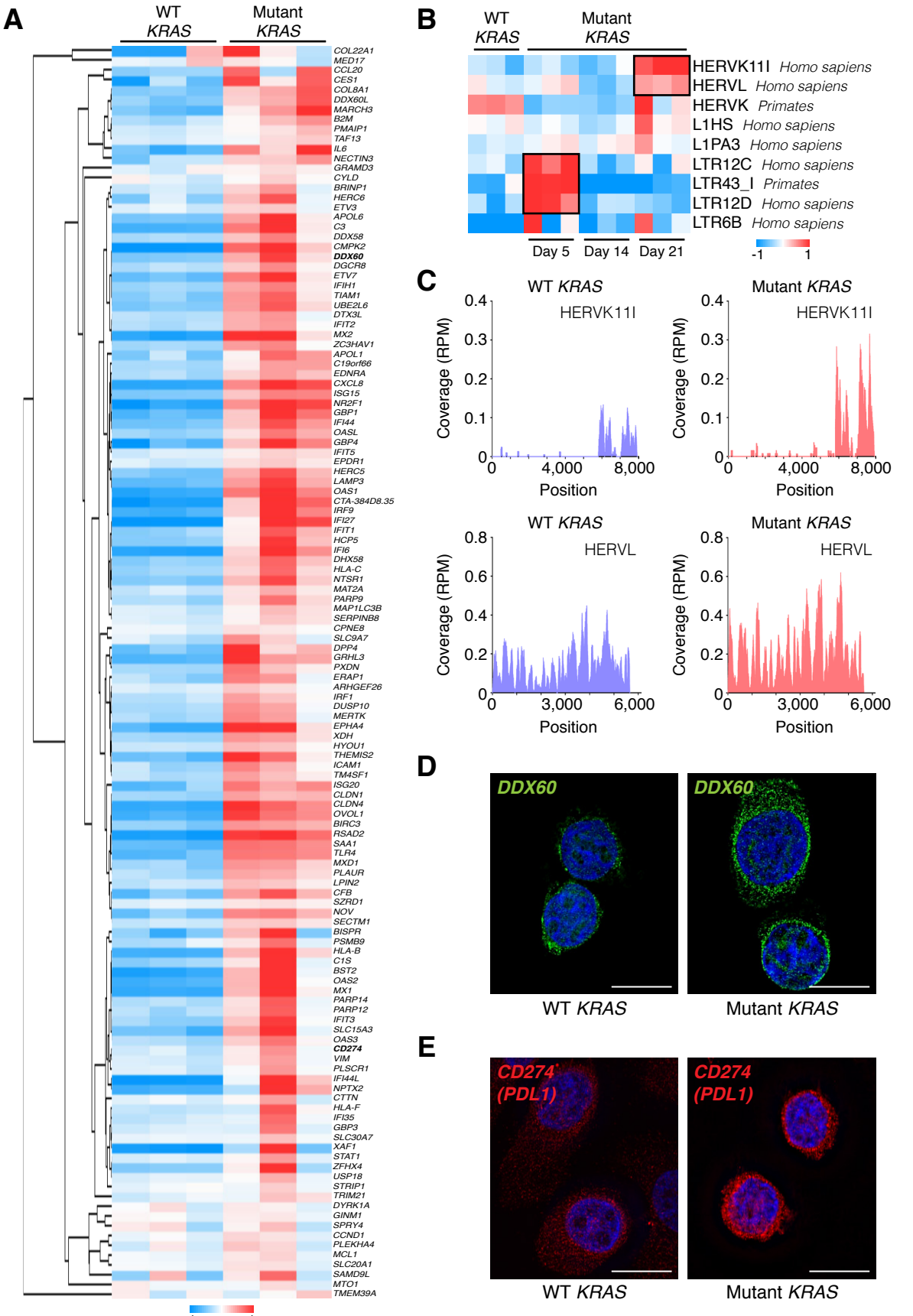
A
WT KRAS
Mutant KRAS
COL22A1
MED17
CCL20
CES1
COL8A1
DDX60L
MARCH3
B2M
PMAIP1
TAF13
IL6
NECTIN3
GRAMD3
CYLD
BRINP1
HERC6
ETV3
APOL6
C3
DDX58
CMPK2
DDX60
DGCR8
ETV7
IFIH1
TIAM1
UBE2L6
DTX3L
IFIT2
MX2
ZC3HAV1
APOL1
C19orf66
EDNRA
CXCL8
ISG15
NR2F1
GBP1
IFI44
OASL
GBP4
IFIT5
EPDR1
HERC5
LAMP3
OAS1
CTA-384D8.35
IRF9
IFI27
IFIT1
HCP5
IFI6
DHX58
HLA-C
NTSR1
MAT2A
PARP9
MAP1LC3B
SERPINB8
CPNE8
SLC9A7
DPP4
GRHL3
PXDN
ERAP1
ARHGEF26
IRF1
DUSP10
MERTK
EPHA4
XDH
HYOU1
THEMIS2
ICAM1
TM4SF1
ISG20
CLDN1
CLDN4
OVOL1
BIRC3
RSAD2
SAA1
TLR4
MXD1
PLAUR
LPIN2
CFB
SZRD1
NOV
SECTM1
BISPR
PSMB9
HLA-B
C1S
BST2
OAS2
MX1
PARP14
PARP12
IFIT3
SLC15A3
OAS3
CD274
VIM
PLSCR1
IFI44L
NPTX2
CTTN
HLA-F
IFI35
GBP3
SLC30A7
XAF1
STAT1
ZFHX4
USP18
STRIP1
TRIM21
DYRK1A
GINM1
SPRY4
CCND1
PLEKHA4
MCL1
SLC20A1
SAMD9L
MTO1
TMEM39A
-1
1
B
WT KRAS
Mutant KRAS
HERVK11I Homo sapiens
HERVL Homo sapiens
HERVK Primates
L1HS Homo sapiens
L1PA3 Homo sapiens
LTR12C Homo sapiens
LTR43_I Primates
LTR12D Homo sapiens
LTR6B Homo sapiens
Day 5
Day 14
Day 21
-1
1
C
WT KRAS
HERVK11I
Mutant KRAS
HERVK11I
WT KRAS
HERVL
Mutant KRAS
HERVL
Coverage (RPM)
Position
0
4,000
8,000
3,000
6,000
0.1
0.2
0.3
0.4
0.6
0.8
D
DDX60
DDX60
WT KRAS
Mutant KRAS
E
CD274 (PDL1)
CD274 (PDL1)
WT KRAS
Mutant KRAS

Figure 2

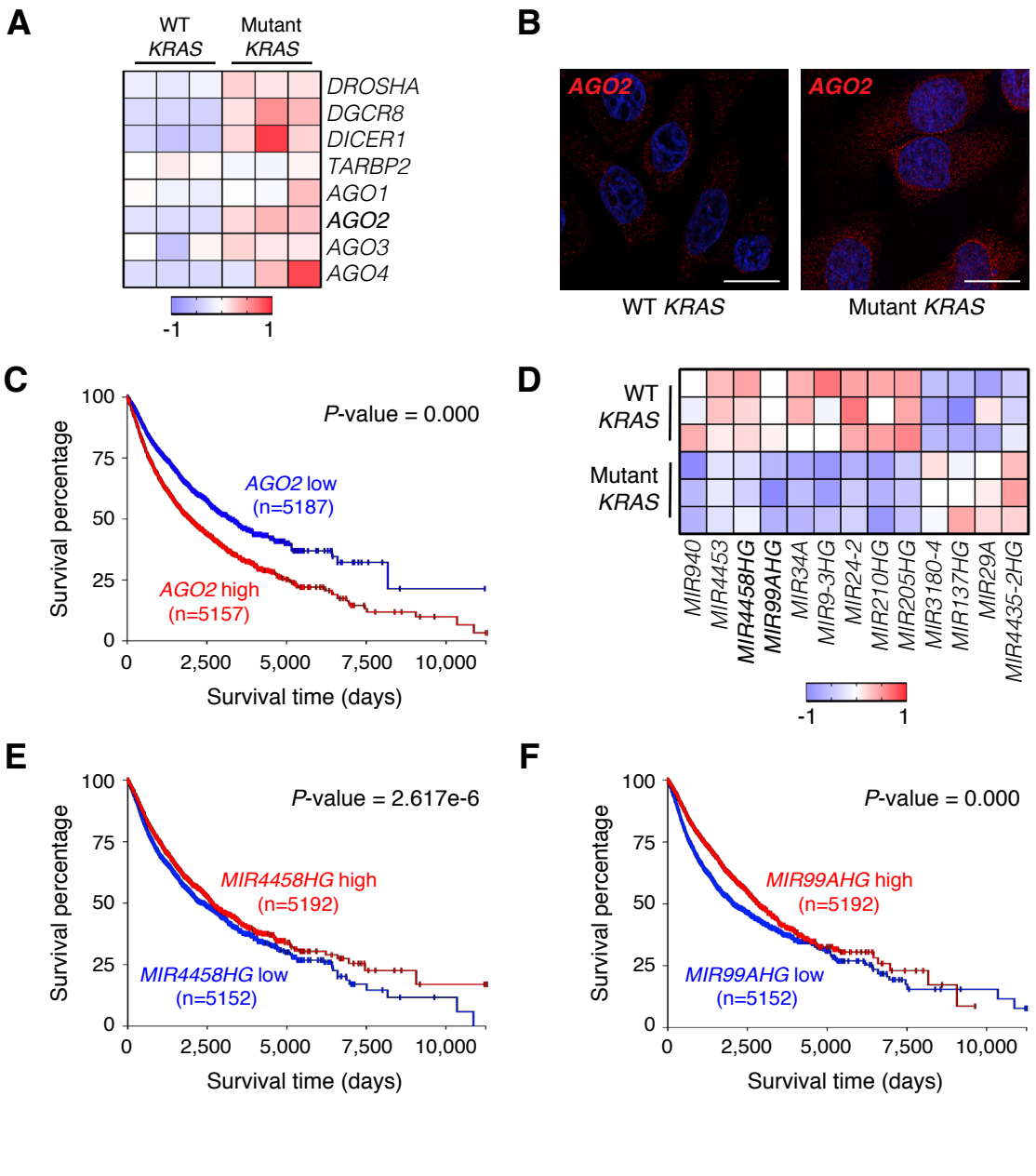
A
WT KRAS
Mutant KRAS
DROSHA
DGCR8
DICER1
TARBP2
AGO1
AGO2
AGO3
AGO4
-1
1
B
AGO2
AGO2
WT KRAS
Mutant KRAS
C
P-value = 0.000
AGO2 low (n=5187)
AGO2 high (n=5157)
Survival percentage
Survival time (days)
D
WT KRAS
Mutant KRAS
MIR940
MIR4453
MIR4458HG
MIR99AHG
MIR34A
MIR9-3HG
MIR24-2
MIR210HG
MIR205HG
MIR3180-4
MIR137HG
MIR29A
MIR4435-2HG
-1
1
E
P-value = 2.617e-6
MIR4458HG high (n=5192)
MIR4458HG low (n=5152)
Survival percentage
Survival time (days)
F
P-value = 0.000
MIR99AHG high (n=5192)
MIR99AHG low (n=5152)
Survival percentage
Survival time (days)

Figure 3

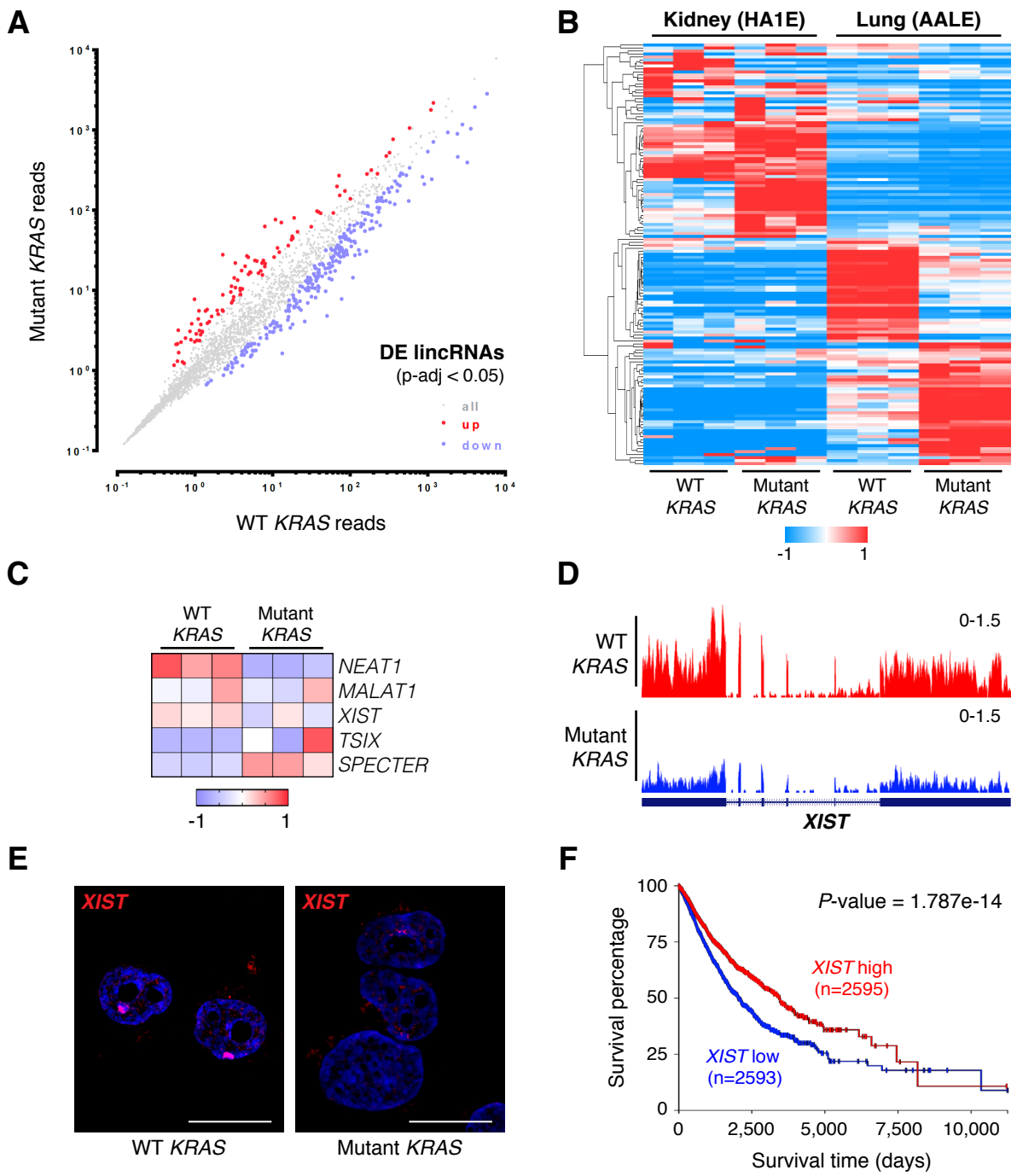
A
Mutant KRAS reads
WT KRAS reads
DE lincRNAs
(p-adj < 0.05)
all
up
down
B
Kidney (HA1E)
Lung (AALE)
WT KRAS
Mutant KRAS
WT KRAS
Mutant KRAS
-1
1
C
WT KRAS
Mutant KRAS
NEAT1
MALAT1
XIST
TSIX
SPECTER
-1
1
D
WT KRAS
0-1.5
Mutant KRAS
0-1.5
XIST
E
XIST
XIST
WT KRAS
Mutant KRAS
F
P-value = 1.787e-14
XIST high
(n=2595)
XIST low
(n=2593)
Survival percentage
Survival time (days)

Figure 4

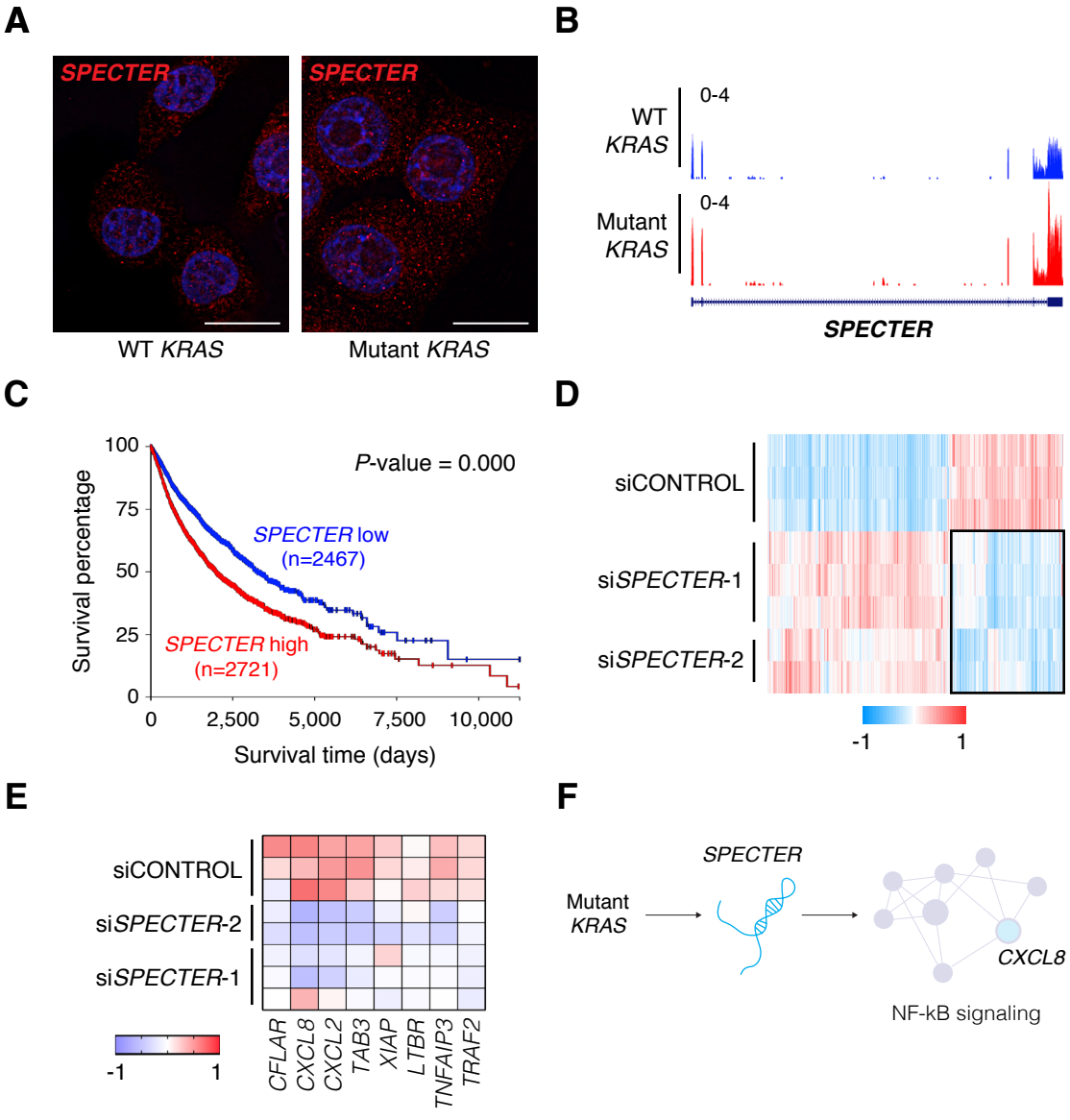
A
SPECTER
SPECTER
WT KRAS
Mutant KRAS
B
WT KRAS
0-4
Mutant KRAS
0-4
SPECTER
C
P-value = 0.000
SPECTER low (n=2467)
SPECTER high (n=2721)
Survival percentage
100
75
50
25
0
0
2,500
5,000
7,500
10,000
Survival time (days)
D
siCONTROL
siSPECTER-1
siSPECTER-2
-1
1
E
siCONTROL
siSPECTER-2
siSPECTER-1
-1
1
CFLAR
CXCL8
CXCL2
TAB3
XIAP
LTBR
TNFAIP3
TRAF2
F
SPECTER
Mutant KRAS
CXCL8
NF-kB signaling

Figure 5

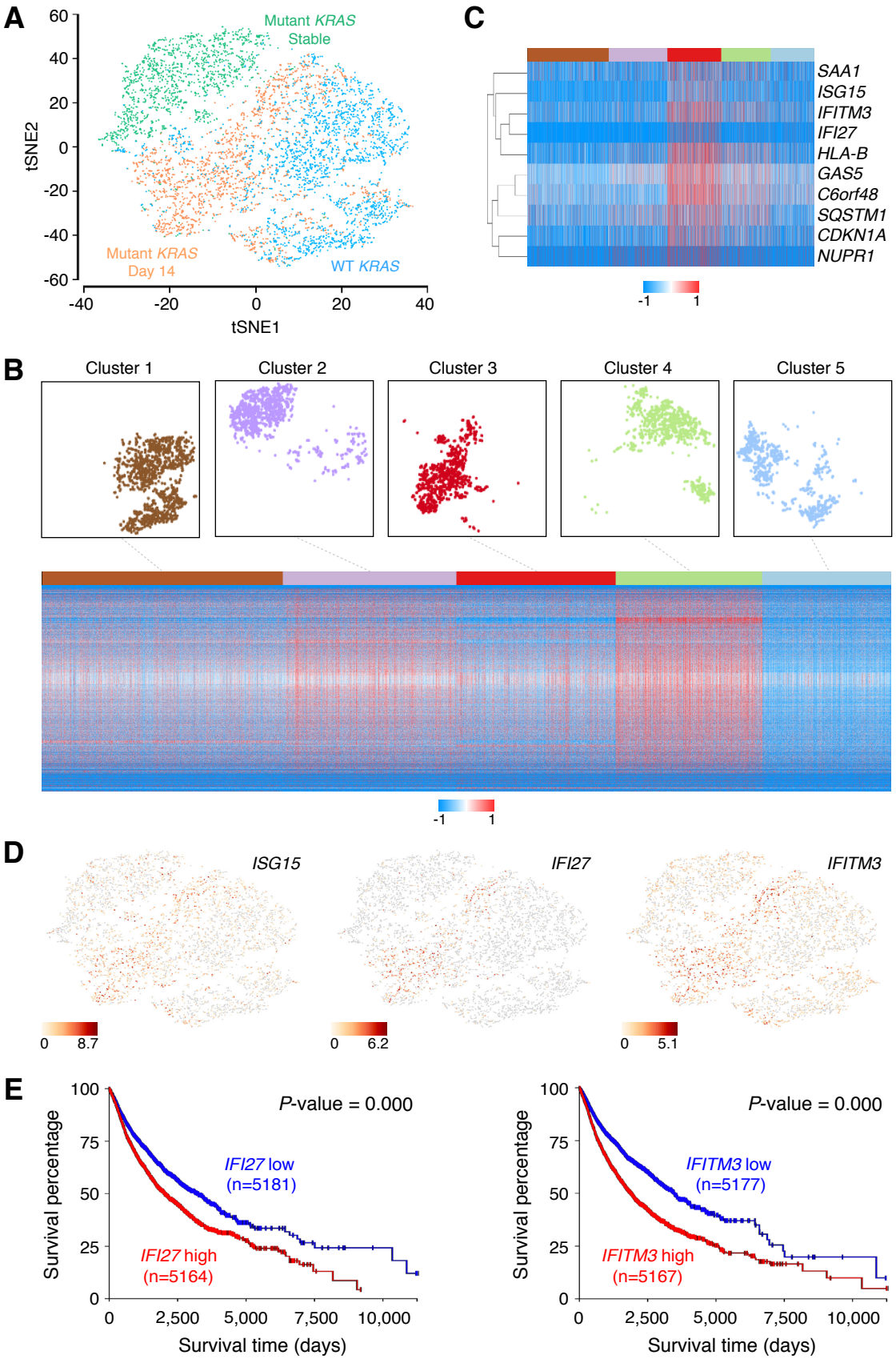
A
Mutant KRAS
Stable
Mutant KRAS
Day 14
WT KRAS
tSNE1
tSNE2
C
SAA1
ISG15
IFITM3
IFI27
HLA-B
GAS5
C6orf48
SQSTM1
CDKN1A
NUPR1
B
Cluster 1
Cluster 2
Cluster 3
Cluster 4
Cluster 5
D
ISG15
IFI27
IFITM3
E
P-value = 0.000
IFI27 low
(n=5181)
IFI27 high
(n=5164)
Survival percentage
Survival time (days)
P-value = 0.000
IFITM3 low
(n=5177)
IFITM3 high
(n=5167)
Survival percentage
Survival time (days)

Figure 6

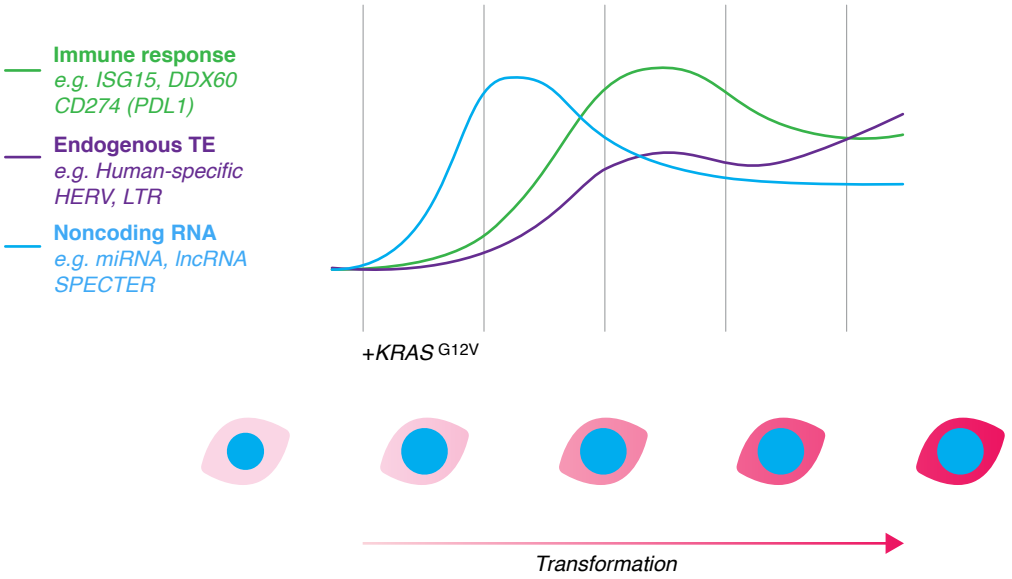
Immune response
e.g. ISG15, DDX60
CD274 (PDL1)
Endogenous TE
e.g. Human-specific
HERV, LTR
Noncoding RNA
e.g. miRNA, lncRNA
SPECTER
+KRAS G12V
Transformation

Figure 7